Numerical and Experimental Assessment of Acoustic Radiation Damping

Suhaib Koji Baydoun and Steffen Marburg

1 Introduction

In the light of the current environmental crisis, lightweight design becomes an increasingly important aspect in various engineering disciplines. Appropriate application of lightweight materials and structures can significantly reduce the energy consumption during manufacturing, operation and recycling of a product. Lightweight structures are characterized by a high stiffness relative to their mass, which however makes them prone to noise, vibration and harshness. In the current engineering practice, vibration mitigation is usually achieved by adding damping treatments in a late stage of the design process or even after manufacturing. The resulting increase in mass and volume can be significant and deteriorates the ecological footprint of the product. Recent approaches for a deliberate introduction of energy dissipation includes materials with high inherent damping [1] and the use of special devices such as particle dampers [2], electrorheological valves [3] and acoustic black holes [4].

This contribution deals with another, often neglected damping phenomenon, commonly denoted as *acoustic radiation damping*. That is the energy dissipation in vibrating structures by virtue of far-field sound radiation, accounting for a significant share in the overall damping of lightweight structures. Although radiation damping is not to be understood as a deliberately introduced damping mechanism, it nevertheless requires accurate quantification. In fact, deliberately introduced treatments require that the extent of added damping is at least within the same order of magnitude as radiation damping in order to be effective [5]. Furthermore, including the effect of radiation damping facilitates more reliable vibroacoustic simulations.

Early attempts to estimate radiation damping are based on the principles of power flow and assume a sufficiently high modal density [6, 7]. While these expressions are accurate approximations in the high frequency range above coincidence [8],

---

S. K. Baydoun (✉) · S. Marburg
TUM School of Engineering and Design, Chair of Vibroacoustics of Vehicles and Machines,
Technical University of Munich, Boltzmannstraße 15, 85748 Garching, Germany
e-mail: suhaib.baydoun@tum.de

P. Eberhard (ed.), *Calm, Smooth and Smart*, Lecture Notes in Applied
and Computational Mechanics 102, https://doi.org/10.1007/978-3-031-36143-2_12

they are rather deficient at low frequencies due to well-separated modes. The latter implies that radiation damping is strongly dependent on the actual excitation and mounting condition of the structure at hand. The applicability of the above mentioned theoretical expressions to complex geometries and to inhomogeneous materials is also difficult to judge. Alternatively, experimental assessment of radiation damping is possible based on sound power measurements inside reverberation chambers and anechoic rooms [9]. This allows to consider geometries that are more complex and also to accurately reflect material properties. If the measurements are conducted in the actual mounting condition, even the effect of the boundary conditions is realistically included. However, in the low frequency range, reliable acoustic measurements are hardly possible due to the modal behavior of the rooms [10].

This contribution presents a framework for a low frequency assessment of radiation damping by acoustic simulations based on the boundary element method (BEM) [11]. The use of BEM yields clear advantages compared to other approaches for evaluating sound radiation and associated damping. Where domain-based discretization methods such as the finite element method (FEM) [12] necessitate special treatments for truncating the far-field sound radiation [13], modeling in BEM is restricted to the radiating surface of the structure. Moreover, compared to the above mentioned experimental approaches, which require special facilities with limited scope of application, the applicability of BEM is more versatile allowing to cover a large range of frequencies and geometrical configurations. This contribution combines BEM with both a structural simulation model [8] and with an experimental characterization of structural mobility [14, 15]. Excitation-dependent radiation loss factors as well as modal loss factors that are associated with certain structural modes are derived.

The remainder of the contribution is organized as follows. Section 2 presents the methodological tools for evaluating radiation damping, including BEM, FEM and structural mobility measurements. Section 3 presents an application of these methods to a honeycomb sandwich panel. Finally, the main content and results are summarized in Sect. 4.

2 Methods

This section describes the framework for a numerical and an experimental-numerical assessment of radiation damping. In the upcoming derivations, a harmonic time dependency of $e^{-\mathrm{i}\omega t}$ is assumed, where $\mathrm{i} = \sqrt{-1}$, the angular frequency is $\omega = 2\pi f$ and t denotes the time.

2.1 Boundary Element Method for the Evaluation of Sound Radiation

In this work, the propagation of acoustic waves in the fluid surrounding the structure is modeled by the inhomogeneous Helmholtz equation [16]

$$\Delta p(\mathbf{x}) + \frac{\omega^2}{c^2} p(\mathbf{x}) = -q, \tag{1}$$

in which c is the speed of sound and q refers to the source. The sound pressure field $p(\mathbf{x})$ is the sum of the scattered field p^{s} and the incident field p^{i}. The same applies to the fluid particle velocity v_{f}, i.e.

$$p(\mathbf{x}) = p^{\mathrm{s}}(\mathbf{x}) + p^{\mathrm{i}}(\mathbf{x}) \tag{2}$$

$$v_{\mathrm{f}}(\mathbf{x}) = v_{\mathrm{f}}^{\mathrm{s}}(\mathbf{x}) + v_{\mathrm{f}}^{\mathrm{i}}(\mathbf{x}). \tag{3}$$

Reformulation of Eq. (1) by the Kirchoff integral theorem and collocation discretization using boundary elements yields the linear system of equations [16]

$$\mathbf{H}(\omega)\mathbf{p} = \mathbf{G}(\omega)\left(\mathbf{v}_{\mathrm{f}} - \mathbf{v}_{\mathrm{f}}^{\mathrm{i}}\right) + \mathbf{H}(\omega)\mathbf{p}^{\mathrm{i}} \tag{4}$$

for the description of the acoustic field. Therein, $\mathbf{p}$ is the unknown vector containing the sound pressure solution at the nodes. The frequency dependent coefficient matrices $\mathbf{H}(\omega)$ and $\mathbf{G}(\omega)$ relate the fluid particle velocity $\mathbf{v}_{\mathrm{f}}$ to the sound pressure. Acoustically rigid baffles can be taken into account by evaluating $\mathbf{H}(\omega)$ and $\mathbf{G}(\omega)$ using a half-space formulation with a modified Green's function [17]. The incident sound pressure field is denoted by $\mathbf{p}^{\mathrm{i}}$ and the corresponding incident particle velocity is $\mathbf{v}_{\mathrm{f}}^{\mathrm{i}}$.

After solving Eq. (4), the time-averaged radiated sound power can be obtained from

$$P = \frac{1}{2}\mathrm{Re}\left(\mathbf{p}^{\mathrm{T}}\boldsymbol{\Theta}\mathbf{v}_{\mathrm{f}}^{*}\right), \tag{5}$$

where $(\cdot)^*$ denotes the conjugate complex, $(\cdot)^{\mathrm{T}}$ is the transpose, and $\boldsymbol{\Theta}$ is the boundary mass matrix, which is obtained by integration of the boundary element interpolation functions. Note that only the real part $\mathrm{Re}\,(\cdot)$ of the complex sound power is associated with radiation damping. The imaginary part of the sound power corresponds to near-field sound radiation, which has a mass-like effect on the structure and hence, does not dissipate energy.

2.2 Numerical Assessment of Radiation Damping Using Finite and Boundary Elements

The fluid particle velocity $\mathbf{v}_\mathrm{f}$ in Eqs. (4) and (5) is determined by the oscillations of the solid structure that is submerged by the fluid. The underlying equations of linear time-harmonic elasticity are discretized by finite elements, which yields [18]

$$\left(\mathbf{K} - \mathrm{i}\omega\mathbf{D} - \omega^2\mathbf{M}\right)\mathbf{u} = \mathbf{f}_\mathrm{s} + \mathbf{f}_\mathrm{f}. \tag{6}$$

The vector $\mathbf{u}$ contains the unknown displacement degrees of freedom (DOFs). The matrices $\mathbf{K}$, $\mathbf{D}$, $\mathbf{M}$ are related to the stiffness, damping and mass of the structure. The excitation is a combination of structural forces $\mathbf{f}_\mathrm{s}$ and fluid forces $\mathbf{f}_\mathrm{f}$. The latter acts by virtue of the surrounding acoustic field. This coupling condition and the continuity condition can be expressed as

$$\mathbf{f}_\mathrm{f} = \mathbf{C}_\mathrm{sf}\mathbf{p}, \quad \text{and} \quad \mathbf{v}_\mathrm{f} = -\mathrm{i}\omega\mathbf{C}_\mathrm{fs}\mathbf{u}, \tag{7}$$

in which the matrices $\mathbf{C}_\mathrm{sf}$ and $\mathbf{C}_\mathrm{fs}$ establish the coupling between the structural and the acoustic subdomains [19]. Combining Eqs. (4), (6) and (7) yields the fully coupled structural acoustic system

$$\begin{bmatrix} \mathbf{K} - \mathrm{i}\omega\mathbf{D} - \omega^2\mathbf{M} & -\mathbf{C}_\mathrm{sf} \\ \mathrm{i}\omega\mathbf{G}(\omega)\mathbf{C}_\mathrm{fs} & \mathbf{H}(\omega) \end{bmatrix} \begin{bmatrix} \mathbf{u} \\ \mathbf{p} \end{bmatrix} = \begin{bmatrix} \mathbf{f}_\mathrm{s} \\ -\mathbf{G}(\omega)\mathbf{v}_\mathrm{f}^\mathrm{i} + \mathbf{H}(\omega)\mathbf{p}^\mathrm{i} \end{bmatrix}. \tag{8}$$

Forming the Schur complement of $\mathbf{H}(\omega)$ with respect to the block system matrix in Eq. (8) and thereby eliminating the pressure DOFs from Eq. (8) yields

$$\left[\mathbf{K} - \mathrm{i}\omega\mathbf{D} - \omega^2\mathbf{M} + \mathrm{i}\omega\mathbf{C}_\mathrm{sf}\mathbf{H}^{-1}(\omega)\mathbf{G}(\omega)\mathbf{C}_\mathrm{fs}\right]\mathbf{u} = \underbrace{\mathbf{f}_\mathrm{s} + \mathbf{C}_\mathrm{sf}\left(\mathbf{p}^\mathrm{i} - \mathbf{H}^{-1}(\omega)\mathbf{G}(\omega)\mathbf{v}_\mathrm{f}^\mathrm{i}\right)}_{\mathbf{f}_\mathrm{t}}, \tag{9}$$

which can be interpreted as a structural equation with an additional term corresponding to the mass and damping contributions of the fluid. The total force vector $\mathbf{f}_\mathrm{t}$ in Eq. (9) comprises both, structural loading $\mathbf{f}_\mathrm{s}$ and acoustic loading due to the incident acoustic field characterized by $\mathbf{p}^\mathrm{i}$ and $\mathbf{v}_\mathrm{f}^\mathrm{i}$. Efficient strategies for solving equations of form (9) are discussed in e.g. [20–22].

2.2.1 Harmonic Radiation Loss Factors

Harmonic radiation loss factors are a result of a frequency-wise response analysis and thus depend on the type of the excitation. They are obtained by relating the time-averaged radiated sound power P obtained by Eq. (5) to the time-averaged total energy E_tot of the vibration [23], i.e.

$$\eta_{\mathrm{r}} = \frac{P}{|\omega E_{\mathrm{tot}}|}. \tag{10}$$

In harmonic problems, the time-averaged total vibrational energy in Eq. (10) is equivalent to twice the time-averaged potential energy. This assumption gives [18]

$$E_{\mathrm{tot}} = \frac{1}{2}\mathbf{u}^{\mathrm{T}}\mathbf{K}\mathbf{u}^{*} - \frac{1}{2}\mathbf{f}_{\mathrm{t}}^{\mathrm{H}}\mathbf{u}. \tag{11}$$

The first term in Eq. (11) is the potential energy due to the elastic straining and the second term corresponds to the work done by external forces. The superscript $(\cdot)^{\mathrm{H}}$ indicates the conjugate transpose of a matrix. In view of the balance of forces in Eq. (9), the time-averaged total vibrational energy can alternatively be expressed as twice the sum of time-averaged kinetic and dissipated energies of the structural acoustic system, i.e.

$$E_{\mathrm{tot}} = \frac{1}{2}\mathbf{u}^{\mathrm{T}}\left(\omega^{2}\mathbf{M} + \mathrm{i}\omega\mathbf{D} - \mathrm{i}\omega\mathbf{C}_{\mathrm{sf}}\mathbf{H}^{-1}(\omega)\mathbf{G}(\omega)\mathbf{C}_{\mathrm{fs}}\right)\mathbf{u}^{*}. \tag{12}$$

Besides the inertial and damping terms corresponding to the finite element matrices $\mathbf{M}$ and $\mathbf{D}$, Eq. (12) also includes energy contributions of the acoustic field. The imaginary part of $\mathbf{H}^{-1}(\omega)\mathbf{G}(\omega)$ is associated with the additional mass effect of the fluid, and its real part corresponds to radiation damping.

Since the energy expressions in Eqs. (11) and (12) are fully equivalent to each other, either of them can be employed to evaluate radiation damping by Eq. (10) in the context of a coupled FEM-BEM analysis. In practice, the expression based on the potential energy in Eq. (11) is more efficient to evaluate since it only comprises sparse coefficient matrices.

2.2.2 Modal Radiation Loss Factors

While the harmonic loss factor given by Eq. (10) depends on the type of the excitation, an alternative measure for radiation damping can be derived based on a modal analysis of the structural acoustic system. Modal analyses of closed acoustic cavities can be solved using FEM [24] or frequency independent BEM formulations [25]. These techniques yield linear eigenvalue problems (EVPs) for which well-established algorithms are available [26]. The situation is different in the context of exterior acoustic domains, which are the relevant case for the analysis of radiation damping. When using the coupled FEM-BEM formulation as described in this contribution, the underlying EVP is obtained by setting the right-hand side of Eq. (9) to zero, i.e.

$$\underbrace{\left[\mathbf{K} - \mathrm{i}\tilde{\omega}\mathbf{D} - \tilde{\omega}^{2}\mathbf{M} + \mathrm{i}\tilde{\omega}\mathbf{C}_{\mathrm{sf}}\mathbf{H}^{-1}(\tilde{\omega})\mathbf{G}(\tilde{\omega})\mathbf{C}_{\mathrm{fs}}\right]}_{\mathbf{A}(\tilde{\omega})}\boldsymbol{\Psi} = \mathbf{0}, \tag{13}$$

in which the vector $\boldsymbol{\Psi}$ denotes a fluid-loaded displacement mode. Equation (13) is a nonlinear EVP, since the coefficient matrices $\mathbf{H}(\tilde{\omega})$ and $\mathbf{G}(\tilde{\omega})$ implicitly depend on the eigenvalue parameter $\tilde{\omega}$. Recent approaches for solving nonlinear EVPs of the form (13) are based on contour integration [27, 28] and on rational approximations [29]. In this contribution, the block SS contour integral method [8] is employed, which essentially transforms the nonlinear EVP (13) into a generalized EVP

$$\mathbf{H}_1 \boldsymbol{\psi} = \lambda \mathbf{H}_2 \boldsymbol{\psi}, \tag{14}$$

with the eigenvector $\boldsymbol{\psi}$ and eigenvalue λ. The latter is identical to the complex eigenfrequency $\tilde{\omega}$ of the structural acoustic system in Eq. (13). The block matrices $\mathbf{H}_1, \mathbf{H}_2 \in \mathbb{C}^{KL \times KL}$ are defined as

$$\mathbf{H}_1 = \begin{bmatrix} \mathbf{M}_0 & \mathbf{M}_1 & \cdots & \mathbf{M}_{K-1} \\ \mathbf{M}_1 & & & \vdots \\ \vdots & & & \mathbf{M}_{2K-3} \\ \mathbf{M}_{K-1} & \cdots & \mathbf{M}_{2K-3} & \mathbf{M}_{2K-2} \end{bmatrix}, \quad \mathbf{H}_2 = \begin{bmatrix} \mathbf{M}_1 & \mathbf{M}_2 & \cdots & \mathbf{M}_K \\ \mathbf{M}_2 & & & \vdots \\ \vdots & & & \mathbf{M}_{2K-2} \\ \mathbf{M}_K & \cdots & \mathbf{M}_{2K-2} & \mathbf{M}_{2K-1} \end{bmatrix}, \tag{15}$$

where K and L are positive integers and need to be set by the user. The product KL determines the subspace dimension. The moments $\mathbf{M}_l \in \mathbb{C}^{L \times L}$ are obtained from

$$\mathbf{M}_l = \frac{1}{2\pi \mathrm{i}} \oint_C z^l \mathbf{U}^{\mathrm{H}} \mathbf{A}^{-1}(z) \mathbf{V} \, \mathrm{d}z, \quad l = 0,...,2K-1, \tag{16}$$

where the matrices $\mathbf{U}$ and $\mathbf{V}$ contain random source vectors as columns. The original system $\mathbf{A}$ is evaluated at the complex-valued shifts z. The latter is defined along an elliptic contour C that has its major axis aligned with the real axis of the complex plane. The two vertices on the real axis correspond to the lower and upper frequency bounds $(f_{\min}, f_{\max})$ respectively. A suitable definition of an ellipse can be given as

$$z(\theta) = \gamma + \rho \left(\cos\theta + \mathrm{i}\zeta \sin\theta\right), \quad \theta \in [0, 2\pi), \tag{17}$$

where $\gamma = (f_{\max} + f_{\min})/2$ and $\rho = (f_{\max} - f_{\min})/2$. After solving the generalized EVP (14), the fluid-loaded structural modes are obtained from $\boldsymbol{\Psi} = \mathbf{S}\boldsymbol{\psi}$. With the definition in Eq. (17) at hand, approximations of the matrices $\mathbf{M}_l$ and $\mathbf{S} = \left[\mathbf{S}_0,...,\mathbf{S}_{K-1}\right]$ can be computed using the N-point trapezoidal rule, i.e.

$$\hat{\mathbf{S}}_l = \frac{1}{\mathrm{i}N} \sum_{j=1}^{N} \left(\frac{z(\theta_j) - \gamma}{\rho}\right)^l z'(\theta_j) \mathbf{A}^{-1} z(\theta_j) \mathbf{V}, \quad \hat{\mathbf{M}}_l = \mathbf{U}^{\mathrm{H}} \hat{\mathbf{S}}_l, \tag{18}$$

where N denotes the number of integration points on the contour and $\theta_j = 2\pi(j-1)/N,\ j = 1,...,N$. The block matrices are assembled according to Eq. (15) using the approximated moments $\hat{\mathbf{M}}_l$. Finally, the generalized EVP $\hat{\mathbf{H}}_1 \hat{\boldsymbol{\psi}}_j = \hat{\lambda}_j \hat{\mathbf{H}}_2 \hat{\boldsymbol{\psi}}_j$ can be solved and the eigenfrequencies $\tilde{\omega}_j$ as well as the fluid-loaded modes $\boldsymbol{\Psi}_j$, $j = 1,\ldots,KL$ can be obtained by

$$\tilde{\omega}_j = \gamma + \rho\hat{\lambda}_j, \quad \boldsymbol{\Psi}_j = \hat{\mathbf{S}}\hat{\boldsymbol{\psi}}_j. \tag{19}$$

The modal loss factor corresponding to a structural mode $\boldsymbol{\Psi}_j$ is determined by [5]

$$\eta_j = -2\frac{\mathrm{Im}\left(\tilde{\omega}_j\right)}{\mathrm{Re}\left(\tilde{\omega}_j\right)}. \tag{20}$$

Note that $\mathrm{Im}\left(\tilde{\omega}_j\right)$ is negative since the harmonic time dependency is defined as $e^{-\mathrm{i}\omega t}$. Assuming $\mathbf{D} = \mathbf{0}$, the modal loss factor in Eq. (20) quantifies the extent of radiation damping for the corresponding fluid-loaded structural mode, since the energy dissipation due to sound radiation is the only damping contribution. In that case, the modal loss factor in Eq. (20) is equivalent to the harmonic loss factor given by Eq. (10) at the respective eigenfrequency $f_j = \mathrm{Re}\left(\tilde{\omega}_j\right)/2\pi$, assuming that the respective mode is excited in the response analysis.

2.3 Hybrid Experimental-Numerical Assessment of Radiation Damping

While the above described coupled FEM-BEM approach facilitates an accurate representation of the acoustic conditions and associated effects such as scattering and short-circuiting in the low frequency range, it suffers from two disadvantages when compared to an experimental evaluation of sound radiation. First, finite element models usually introduce vast simplifications of boundary conditions such as *clamped* or *simply supported*, which can yield large errors in acoustic quantities when sound radiation is mainly induced by edge and corner motions [23]. Second, vibroacoustic behavior is largely determined by the elastic material properties of the structure at hand. It is clear that accurate predictions of radiation damping therefore demand precise material models. Ironically, radiation damping is particularly relevant in complex material configurations that are designed to achieve a high ratio of bending stiffness to mass. These issues can be addressed by a hybrid experimental-numerical method developed in [15]. It is briefly reproduced below.

The structural finite element model is omitted and instead, the structure is characterized by

$$\mathbf{v}_\mathrm{r} = \mathbf{Y}(\omega)\left[\mathbf{f}_\mathrm{e} + \mathbf{C}_\mathrm{ef}\left(\mathbf{p}^\mathrm{i} - \mathbf{H}^{-1}(\omega)\mathbf{G}(\omega)\mathbf{v}_\mathrm{f}^\mathrm{i}\right)\right], \tag{21}$$

in which $\mathbf{Y}(\omega)$ is a mobility matrix containing experimentally determined transfer functions that relate the force excitation to the surface velocity. The vector $\mathbf{v}_\mathrm{r}$ contains the surface velocities at the nodes of the response grid. The excitation vector in square brackets on the right-hand side of Eq. (21) comprises structural excitation $\mathbf{f}_\mathrm{e}$ as well as excitation by an incident acoustic field. The excitation vector is defined on a (possibly different) excitation grid. The force associated with the incident acoustic field is computed by BEM resulting in a similar expression for the force vector as on the right-hand side of Eq. (9). Having evaluated $\mathbf{v}_\mathrm{r}$ for a given excitation, the particle velocities on the nodes of the boundary element model are computed by

$$\mathbf{v}_\mathrm{f} = \mathbf{C}_\mathrm{fr}\mathbf{v}_\mathrm{r}, \tag{22}$$

and the pressure field and sound radiation can be obtained by Eqs. (4) and (5). The coupling matrix $\mathbf{C}_\mathrm{ef}$ in Eq. (21) relates the acoustic quantities on the boundary element mesh to the excitation grid, and similarly, $\mathbf{C}_\mathrm{fr}$ in Eq. (22) establishes the coupling between the response grid and the boundary element nodes.

In order to assess radiation damping via Eq. (10), the time-averaged total vibrational energy is evaluated by

$$E_\mathrm{tot} = \frac{1}{2}\mathbf{v}_\mathrm{r}^\mathrm{T}\left(\mathbf{M}_\mathrm{r} - \frac{\mathrm{i}}{\omega}\mathbf{C}_\mathrm{rf}\mathbf{H}^{-1}(\omega)\mathbf{G}(\omega)\mathbf{C}_\mathrm{fr}\right)\mathbf{v}_\mathrm{r}^*, \tag{23}$$

which is similar to the expression in Eq. (12). The mass matrix $\mathbf{M}_\mathrm{r}$ of the structure under test is assembled by the structural mass contributions of each element on the response grid. In this work, the transfer functions contained in $\mathbf{Y}(\omega)$ are obtained by scanning laser Doppler vibrometry (LDV) and excitation by an automated modal hammer. In many situations, it is not necessary to have the whole matrix $\mathbf{Y}(\omega)$, e.g. when only a local excitation is of interest. Moreover, symmetry of the structure and boundary conditions can be exploited to reduce the measurement effort. Details on this hybrid experimental-numerical approach are given in [15]. The experimental procedure for determining the mobility matrix $\mathbf{Y}(\omega)$ is reported in Sect. 3.2.

3 Application

This section studies the acoustic radiation damping of a honeycomb sandwich panel using the described numerical as well the hybrid experimental-numerical method. Modal and harmonic loss factors for different types of excitations and acoustic boundary conditions are computed.

The panel consists of two aluminum face sheets enclosing an aluminum honeycomb core. The dimension and the material properties are listed in Table 1. Two different load cases are considered. A point force is located at ($x = 0.062\,\mathrm{m},\ y = 0.188\,\mathrm{m}$) and a monopole sound source is located at ($x = 1.376\,\mathrm{m},\ y = 1.25\,\mathrm{m},\ z = 0.3\,\mathrm{m}$). The origin of the corresponding coordinate system coincides with the center of the panel.

Table 1 Geometry and material properties of the aluminum honeycomb sandwich panel provided by the manufacturer. Assumed values are marked with a star*

Aluminum face sheets		
Thickness	t	0.5 mm
Density	ρ_f	2690 kg/m^3
Young's modulus	E	70 GPa
Poisson's ratio	ν_a	0.3
Aluminum honeycomb core		
Thickness	h	4.5 mm
Density	ρ_c	135 kg/m^3
Young's modulus	E_x, E_y	10 MPa*
Young's modulus	E_z	360 MPa
Shear modulus	G_{xy}	1 MPa*
Shear modulus	G_{yz}	280 MPa
Shear modulus	G_{xz}	140 MPa
Poisson's ratio	ν_c	0.01*
Dimensions	$l_x \times l_y$	0.748 × 0.5 m^2

3.1 Results Obtained by Coupled Finite and Boundary Element Analyses

In this section, radiation damping of the sandwich panel is studied using the coupled FEM-BEM framework described in Sect. 2.1. The panel itself is modeled using twenty-noded hexahedral solid finite elements for the representation of the core and eight-noded quadrilateral shell finite elements based on the Reissner-Mindlin theory for the two face sheets. A uniform mesh of 36 × 24 elements along the in-plane directions ensures that at least six elements capture one bending wave length in the considered frequency range. A single solid element is used to discretize the core in the out-of-plane direction. Simply supported boundary conditions are applied to the two short edges of the panel. The long edges are unconstrained. Structural damping is neglected in the following. Figure 1 shows the finite element mesh of the panel with the position of the point force excitation.

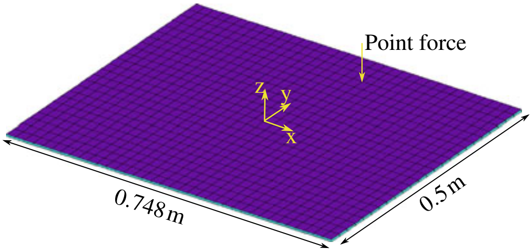

Fig. 1 Finite element model of the sandwich panel

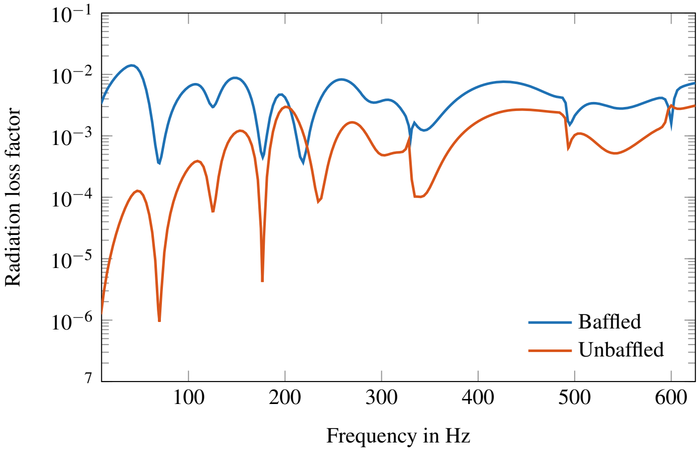

Fig. 2 Radiation loss factor by harmonic response of the honeycomb sandwich panel subject to excitation by a point force. Comparison between baffled and unbaffled acoustic boundary conditions

The structural finite element mesh is coupled to a boundary element model for the representation of the surrounding acoustic field. The boundary elements coincide with the finite elements. Two different acoustic conditions are studied: First, the panel is confined in an infinitely extended baffle, which prohibits acoustic flow between the two sides of the panel. Second, the panel is situated in a free acoustic field, which will be referred to as *unbaffled*.

Figure 2 shows radiation loss factors obtained by harmonic response analyses of the panel subject to excitation by a point force. The frequency range up to 625 Hz is considered. The baffled and the unbaffled cases are compared with each other. The acoustic short circuiting occurring in the unbaffled panel decreases radiation efficiency and thus radiation damping at low frequencies. The two curves converge to each other towards higher frequencies. The apparent dips in the loss factors correspond to structural modes of the panel associated with sound pressure cancellation among neighboring half-cells. This cancellation effect disappears at higher frequencies.

Besides harmonic analyses, modal analyses of the air-loaded panel are performed using the algorithm described in Sect. 2.2.2. Thirteen eigenfrequencies occur in the considered frequency range. The resulting modal radiation loss factors are obtained by Eq. (20) and plotted in Figs. 3 and 4 for the baffled and unbaffled case, respectively. In addition, harmonic radiation loss factors for both point force excitation and excitation by a monopole source are shown. The latter yields significantly higher loss factors at frequencies between resonances due the spatially uniform loading. At the eigenfrequencies, however, the harmonic loss factors of the two load cases consistently agree with each other. They coincide with the modal radiation loss factors, which are inherent properties of the structural acoustic system and independent of the excitation.

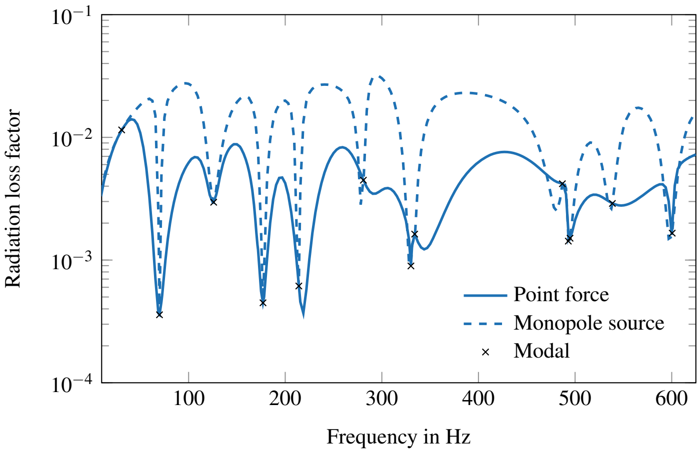

Fig. 3 Radiation loss factor of the honeycomb sandwich panel confined in an acoustically rigid baffle. Comparison between point force excitation and excitation by a monopole source. Additionally, the modal radiation loss factors are plotted at their respective eigenfrequencies

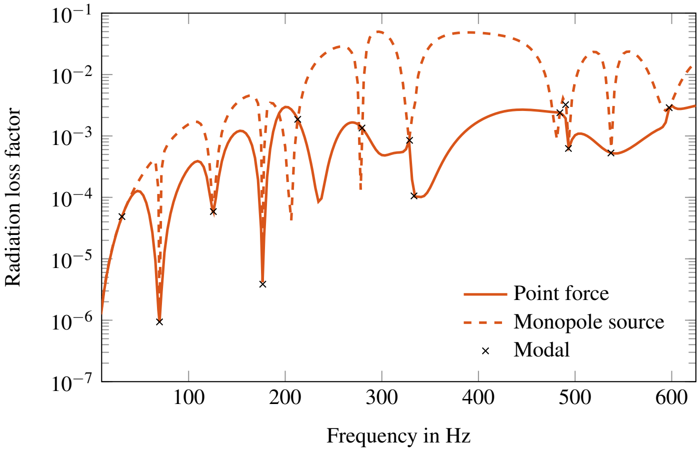

Fig. 4 Radiation loss factor of the unbaffled honeycomb sandwich panel. Comparison between point force excitation and excitation by a monopole source. Additionally, the modal radiation loss factors are plotted at their respective eigenfrequencies

Table 2 lists the eigenfrequencies of the panel in vacuo as well as the eigenfrequencies resulting from a modal analysis including air loading for the baffled and the unbaffled case. Eigenfrequency shifts of up to 5 % for the baffled and the unbaffled panel clearly illustrate the effect of additional mass and damping due to the acoustic field.

Table 2 Eigenfrequencies of the honeycomb sandwich panel in vacuo and in air considering baffled and unbaffled acoustic boundary conditions

No.	In Vacuo	Baffled (%)	Unbaffled (%)
1	32.7 Hz	30.7 Hz (−5.9)	31.0 Hz (−5.0)
2	70.7 Hz	69.9 Hz (−2.6)	69.9 Hz (−2.5)
3	130 Hz	126 Hz (−3.2)	126 Hz (−3.5)
4	181 Hz	177 Hz (−2.1)	177 Hz (−2.2)
5	218 Hz	214 Hz (−1.8)	213 Hz (−2.3)
6	287 Hz	281 Hz (−2.2)	279 Hz (−2.7)
7	336 Hz	330 Hz (−1.7)	329 Hz (−2.1)
8	340 Hz	334 Hz (−1.8)	333 Hz (−2.0)
9	498 Hz	487 Hz (−1.7)	484 Hz (−2.3)
10	501 Hz	493 Hz (−1.6)	490 Hz (−2.1)
11	503 Hz	495 Hz (−1.6)	493 Hz (−2.0)
12	547 Hz	540 Hz (−1.6)	537 Hz (−1.8)
13	610 Hz	539 Hz (−1.6)	598 Hz (−2.0)

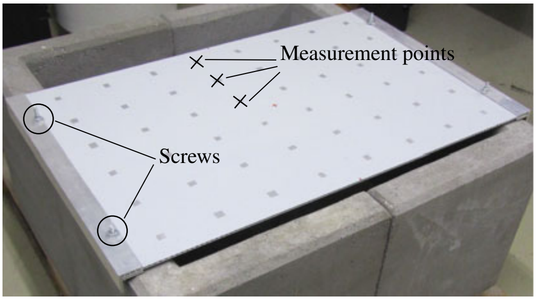

Fig. 5 Set-up of the honeycomb sandwich panel for mobility measurements

3.2 Results Obtained by the Hybrid Procedure

The finite element model of the sandwich panel is now replaced by measured mobility data of the panel in order to apply the hybrid procedure described in Sect. 2.3 for the assessment of radiation damping. The sandwich panel is mounted onto a concrete foundation by gluing the short edges of the panel into aluminum F-profiles and fixing them with screws. The set-up is shown in Fig. 5. The excitation is carried out on a uniform grid with 6×4 patches by means of an automated modal hammer (NV Tech SAM1). The force transmitted at the hammer tip is measured in order to derive the respective transfer functions.

On the opposite side of the panel, scanning LDV (Polytec PSV 500) is performed on a uniform response grid of 8×6 patches in order to measure the surface vibrations of the panel. The signal to noise ratio is increased by applying reflective tape at the laser positions. The resulting transfer function matrix $\mathbf{Y}(\omega)$ is of size 48×24.

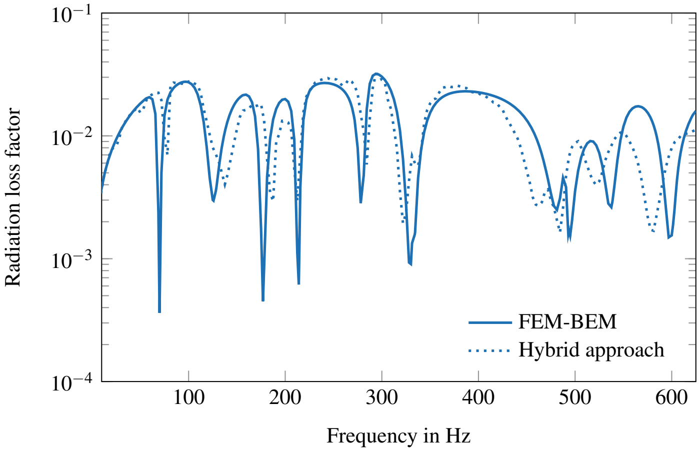

Fig. 6 Radiation loss factor of the baffled honeycomb sandwich panel subject to excitation by a monopole sound source. Comparison between the results obtained by the FEM-BEM approach and the hybrid approach

The transfer functions are obtained by relating the Fourier transforms of the velocity signal to the force signal. The measurement time is long enough so that all signals die out. No window functions are required. Complex frequency domain averaging mitigates the noise that is not phase correlated.

Figures 6 and 7 show the radiation loss factors of the panel in the baffled and unbaffled condition, respectively. An excitation by a monopole sound source is considered. In the hybrid approach, the incident sound field is created using the boundary element model and the resulting force vector is obtained by coupling the boundary element mesh to the experimental excitation grid. The velocity response is then computed by multiplication with the measured matrix of mobilities, c.f. Eq. (21). Finally, the radiated sound field is again computed by BEM.

Figures 6 and 7 and indicate an excellent agreement between the numerical and the hybrid experimental-numerical approach. The numerically predicted eigenfrequencies match the experimental results well, which suggests that the simply supported boundary conditions in the finite element model are a reasonable approximation of the actual mounting condition in the experiment. The material modeling in the structural finite element model also accurately reflects the properties of the sandwich panel. In other cases in which the mounting condition and material properties are subject to uncertainties or prestress occurs during manufacturing, the hybrid approach facilitates an accurate low frequency assessment of radiation damping [15].

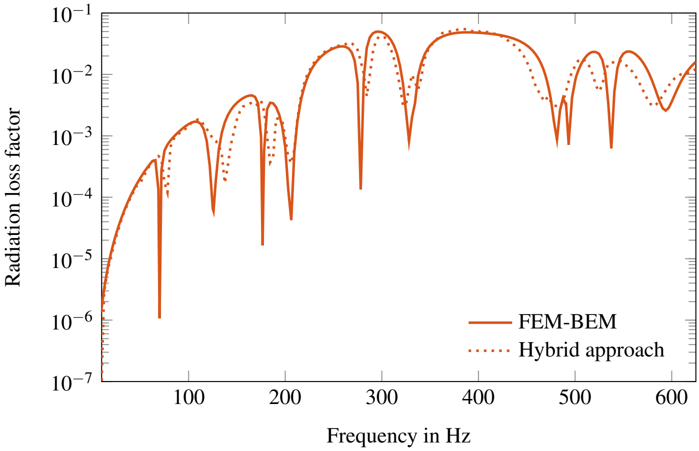

Fig. 7 Radiation loss factor of the unbaffled honeycomb sandwich panel subject to excitation by a monopole sound source. Comparison between the results obtained by the FEM-BEM approach and the hybrid approach

4 Summary and Conclusion

This contribution has reviewed two recent approaches for assessing acoustic radiation damping in the low frequency range. The methodological basis for both approaches is the acoustic BEM, which allows to predict the radiated sound power of structures exhibiting complex geometrical configurations and acoustic boundary conditions.

The first approach is purely numerical and employs a finite element model to characterize the vibrational behavior of the submerged solid structure. Harmonic radiation loss factors are derived based on the forced response of the coupled structural acoustic system. In addition, excitation-independent modal radiation loss factors are obtained by solving the underlying nonlinear structural acoustic eigenvalue problem by a contour integral method.

The second approach is based on an experimentally obtained matrix of mobilities. The mobility matrix, which contains rtransfer functions relating the surface velocity to the force excitation, is coupled to a numerical model of the surrounding acoustic field based on BEM. This approach allows consideration of the actual mechanical boundary conditions and elastic material properties without the need of acoustic measurement facilities.

The two approaches were used to analyze the radiation damping of a honeycomb sandwich panel. The results illustrate the pronounced influence of the type of excitation and acoustic boundary conditions on radiation damping in the low frequency range. At the structural resonance frequencies, however, the harmonic radiation loss factors consistently agree with the excitation-independent modal loss factors. The hybrid experimental-numerical method has achieved excellent agreement with the numerically predicted results. The results in [15, 29] indicate that the methods presented here are also applicable to more complex geometries.

Ongoing and future work includes application of the presented method in the design process of damping treatments and exploitation of radiation damping for deliberate energy dissipation.

Acknowledgements This work was supported by the German Research Foundation (DFG project MA 2395/15-2) in the context of the priority program 1897 “Calm, Smooth and Smart—Novel Approaches for Influencing Vibrations by Means of Deliberately Introduced Dissipation.”

References

1. Ehrig, T., Holeczek, K., Modler, N., Kostka, P.: Dynamic behaviour adaptation of lightweight structures by compressible constrained layer damping with embedded polymeric foams and nonwovens. Appl. Sci. **9**(3), 3490 (2019)
2. Gnanasambandham, C., Fleissner, F., Eberhard, P.: Enhancing the dissipative properties of particle dampers using rigid obstacle-grids. J. Sound Vib. **484**, 115522 (2020)
3. Tan, A.S., Belkner, J., Stroschke, A., Sattel, T.: Damping adjustment utilizing digital electrorheological valves with parallely segmented electrodes. Smart Mater. Struct. **28**(7), 075013 (2019)
4. Meyer, C.H., Lerch, C., Rothe, S., Hoffmann, S., Langer, S.C., Lohmann, B., Rixen, D.J.: Study on model reduction for position optimization of acoustic blackholes. Proc. Appl. Math. & Mech. **21**(1), e202100123 (2021)
5. Mead, D.J.: Passive Vibration Control. John Wiley & Sons Ltd, Chichester, England (1999)
6. Maidanik, G.: Response of ribbed panels to reverberant acoustic fields. J. Acoust. Soc. Am. **34**(6), 809–826 (1962)
7. Crocker, M.J., Price, A.J.: Sound transmission using statistical energy analysis. J. Sound Vib. **9**(3), 469–486 (1969)
8. Baydoun, S.K., Marburg, S.: Investigation of radiation damping in sandwich structures using finite and boundary element methods and a nonlinear eigensolver. J. Acoust. Soc. Am. **147**(3), 2020–2034 (2020)
9. Zhou, R., Crocker, M.J.: Sound transmission loss of foam-filled honeycomb sandwich panels using statistical energy analysis and theoretical and measured dynamic properties. J. Sound Vib. **329**(6), 673–686 (2010)
10. Scrosati, C., Scamoni, F., Bassanino, M., Mussin, M., Zambon, G.: Uncertainty analysis by a Round Robin Test of field measurements of sound insulation in buildings: single numbers and low frequency bands evaluation—Airborne sound insulation. Noise Control. Eng. J. **61**(3), 291–306 (2013)
11. Kirkup, S.: The boundary element method in acoustics: a survey. Appl. Sci. **9**(8), 1642 (2019)
12. Kaltenbacher, M.: Computational Acoustics. Springer, Cham, Switzerland (2018)
13. Astley, R.J., Macaulay, G.J., Coyette, J.-P., Cremers, L.: Three-dimensional wave-envelope elements of variable order for acoustic radiation and scattering. part I. formulation in the frequency domain. J. Acoust. Soc. Am. **103**(1), 49–63 (1998)
14. Roozen, N.B., Leclère, Q., Urbán, D., Méndez Echenagucia, T., Block, P., Rychtáriková, M., Glorieux, C.: Assessment of the airborne sound insulation from mobility vibration measurements; a hybrid experimental numerical approach. J. Sound Vib. **432**, 680–698 (2018)
15. Baydoun, S.K., Roozen, N.B., Marburg, S.: Hybrid assessment of acoustic radiation damping combining in-situ mobility measurements and the boundary element method. Acta Acust. **6**, 44 (2022)

16. Marburg, S., Nolte, B.: A unified approach to finite and boundary element discretization in linear time-harmonic acoustics. In: Marburg, S., Nolte, B. (eds.) Computational Acoustics of Noise Propagation in Fluids. Finite and Boundary Element Methods, pp. 1–34. Springer (2008)
17. Ochmann, M., Brick, H.: Acoustical radiation and scattering above an impedance plane. In: Marburg, S., Nolte, B. (eds.) Computational Acoustics of Noise Propagation in Fluids. Finite and Boundary Element Methods, pp. 459–494. Springer (2008)
18. Bathe, K.-J.: Finite Element Procedures. Englewood Cliffs, New Jersey: Prentice Hall (1996)
19. Peters, H., Marburg, S., Kessissoglou, N.: Structural-acoustic coupling on non-conforming meshes with quadratic shape functions. Int. J. Numer. Methods Eng. **91**(1), 27–38 (2012)
20. Baydoun, S.K., Voigt, M., Jelich, C., Marburg, S.: A greedy reduced basis scheme for multifrequency solution of structural acoustic systems. Int. J. Numer. Methods Eng. **121**(2), 187–200 (2020)
21. Jelich, C., Baydoun, S.K., Voigt, M., Marburg, S.: A greedy reduced basis algorithm for structural acoustic systems with parameter and implicit frequency dependence. Int. J. Numer. Methods Eng. **122**(24), 7409–7430 (2021)
22. Baydoun, S.K., Voigt, M., Marburg, S.: Low-rank iteration schemes for the multi-frequency solution of acoustic boundary element equations. J. Theor. Comput. Acoust. **29**(3), 2150004 (2021)
23. Fahy, F., Gardonio, P.: Sound and Structural Vibration. Academic Press, Oxford, United Kingdom (2007)
24. Petyt, M., Lea, J., Koopmann, G.: A finite element method for determining the acoustic modes of irregular shaped cavities. J. Sound Vib. **45**(4), 495–502 (1976)
25. Banerjee, P.K., Ahmad, S., Wang, H.C.: A new BEM formulation for the acoustic eigenfrequency analysis. Int. J. Numer. Methods Eng. **26**(6), 1299–1309 (1988)
26. Roman, J.E., Campos, C., Romero, E., Tomàs, A.: Slepc users manual. Technical report, Universitat Politècnica de València (2020)
27. Kimeswenger, A., Steinbach, O., Unger, G.: Coupled finite and boundary element methods for fluid-solid interaction eigenvalue problems. SIAM J. Numer. Anal. **52**(5), 2400–2414 (2014)
28. Zheng, C.-J., Bi, C.-X., Zhang, C., Gao, H.-F., Chen, H.-B.: Free vibration analysis of elastic structures submerged in an infinite or semi-infinite fluid domain by means of a coupled FE-BE solver. J. Comput. Phys. **359**, 183–198 (2018)
29. Baydoun, S.K., Voigt, M., Goderbauer, B., Jelich, C., Marburg, S.: A subspace iteration eigensolver based on Cauchy integrals for vibroacoustic problems in unbounded domains. Int. J. Numer. Methods Eng. **122**(16), 4250–4269 (2021)